

Study of Cosmogenic Neutron Backgrounds at LNGS

A. Empl^{*}, R. Jasim, E. Hungerford and P. Mosteiro^a

Department of Physics, University of Houston, Houston, TX 77204

^aDepartment of Physics, Princeton University, Princeton, NJ 08544

Abstract. Cosmic muon interactions are important contributors to backgrounds in underground detectors when searching for rare events. Typically neutrons dominate this background as they are particularly difficult to shield and detect in a veto system. Since actual background data is sparse and not well documented, simulation studies must be used to design shields and predict background rates. This means that validation of any simulation code is necessary to assure reliable results. This work studies the validation of the FLUKA simulation code, and reports the results of a simulation of cosmogenic background for a liquid argon two-phase detector embedded within a water tank and liquid scintillator shielding.

1 Introduction

This paper reports the use of the FLUKA simulation code to study muon-produced, cosmogenic backgrounds at the Italian National Laboratory for Underground Research (LNGS). Care was taken to validate FLUKA with available data, and compare the results of our studies with previous simulations. We are particularly interested in the predicted neutron backgrounds for a dark matter direct detection experiment DarkSide-50, now under construction at the LNGS, and its potential extension to a 3 ton liquid argon two-phase detector. We also report work relating to backgrounds in the nearby Borexino detector, which when this data is available in the near future, will provide substantially better cosmogenic neutron information which can be used to validate further simulations.

Cosmic muon interactions can be important contributors to backgrounds as they may dominate experiments searching for rare events. Typically, such experiments are placed in deep underground facilities where only neutrinos and high energy muons are able to reach the detectors. For example, the first measurement of atmospheric neutrinos was undertaken at the Kolar Gold Fields in 1965 [1]. Muons in particular, induce background rates through showers of secondary particles created in local interactions near the detector, and only high energy muons penetrate to the depth of the experimental halls. Thus the total cosmic muon flux decreases with depth as lower energy muons are removed from the spectrum. However, little experimental information about muon-induced secondaries at depth is available.

Most studies have concentrated on the neutron flux in the muon radiation field,

^{*}Corresponding author, Anton.Empl@mail.uh.edu

since energetic neutrons are difficult to shield and are usually the critical background. However, the low rates and challenges inherent in neutron measurements require careful interpretation of the available data. All measurements of the neutron flux employ liquid scintillation detectors which record the gamma radiation emitted after neutron capture. Obviously detector geometry and efficiencies affect the interpretation of the data, so experiments have to rely on simulations of particle interactions and transport to extract and predict the measured muon-induced backgrounds.

2 FLUKA

2.1 The FLUKA Code

Fluka [2, 3] is a fully integrated particle-physics, Monte Carlo simulation package which traditionally has been applied to problems related to cosmic rays and cosmogenic backgrounds in deep underground experiments. The origin of Fluka however, is linked to shielding designs for particle accelerators, and was started as early as 1962. The modern Fluka code finds many applications ranging from high energy particle physics to medical physics and radio-biology.

Design and development of Fluka has always focused on the implementation and improvement of verified physical models. Thus Fluka adopts microscopic models connected in a way which maintains consistency among all the reaction steps and types. Conservation laws are enforced at each step and predictions are bench-marked against experimental data at the level of single interactions. This results in a consistent approach to all energy/target/projectile combinations with a minimal overall set of free parameters. As a consequence, predictions for complex simulation problems are robust and arise naturally from the underlying physical models, even where no direct experimental data are available [4].

Information about the implemented models is available through the Fluka manual, additional documentation, and lectures located at the official Fluka website [5]. The version of Fluka used for the present study is FLUKA2011.2, from November 2011.

2.2 Relevant code benchmarks

Predictions of backgrounds to rare physics processes at underground facilities depend on the full range of physics implemented in Fluka. To illustrate the quality of Fluka predictions, a few relevant published benchmark comparisons with available experimental data are presented in the following subsections.

2.2.1 Muon-nuclear interactions

Although muon-nuclear interactions at high energies are not well measured, they are implemented in Fluka by photo-nuclear interactions involving virtual photons. The energies relevant to the simulations of interest are approximately 250-300 GeV for single-muon events. Figure 1 shows the results of the CERN muon test beam of 300 GeV incident on a section of the ATLAS tile calorimeter [6]. The energy deposition, resulting from both electromagnetic and hadronic showers, is shown in the figure, and agreement between measurement and simulation is very good. In particular, events with

very large energy deposition in the hadronic calorimeter are well reproduced. For this class of events, hadronic effects become comparable to electromagnetic effects. It should be noted that this agreement is absolute as no relative scaling is applied. The energy scale for both the measurement and the Fluka simulation are derived independently from calibration measurements using a 20-GeV electron beam.

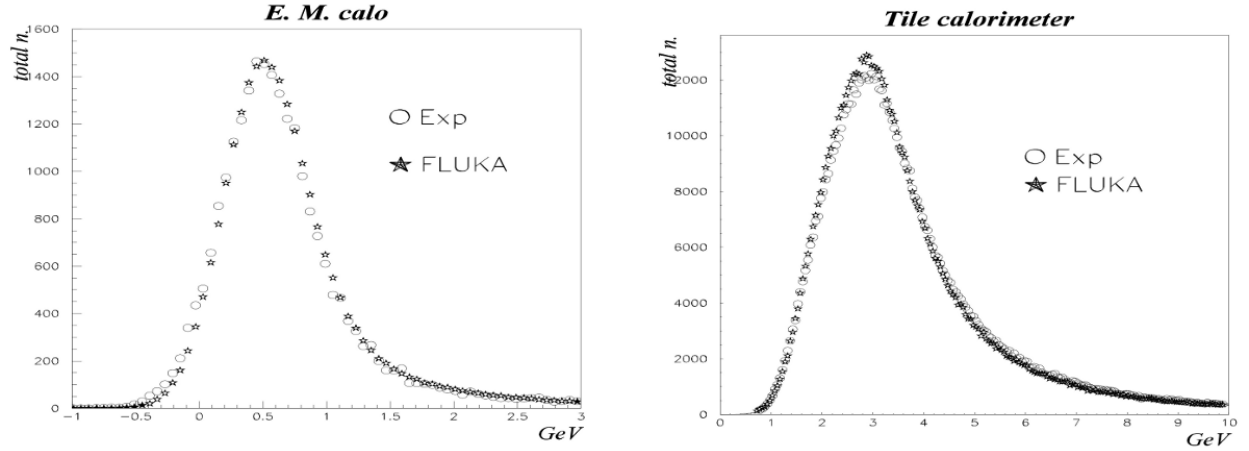


Figure 1: Energy deposition into the electromagnetic (a) and hadronic (b) part of the ATLAS combined calorimeter from a 300-GeV muon test beam at CERN.

2.2.2 Photo-nuclear interactions

Muon-nuclear interactions are treated as virtual photo-nuclear interactions in Fluka. Figure 2b shows the results of a measurement of photo-nuclear reactions on a lead target, $^{208}\text{Pb}(\gamma, x n)$, in the energy range of $20 \text{ MeV} < E < 140 \text{ MeV}$. The cross section for multiple neutron emission as a function of photon energy is also shown. The symbols correspond to experimental data, and the Fluka predictions are lines. The different curves correspond to events with neutron multiplicities $\geq N$, with $2 \leq N \leq 8$, in descending order¹. Data and simulation are in good agreement. See Ref. [7] for more details on the implementation of photo-nuclear interactions in Fluka.

2.2.3 Neutron production and transport

Neutron interaction and transport are important to obtain an accurate simulation of muon-induced neutron backgrounds. The majority of neutrons are produced by secondary processes in hadronic showers. To demonstrate Fluka's capabilities for simulating neutron production and transport, Figure 2a shows the measured and simulated neutron energy spectra for the n_TOF facility[8]. This neutron time-of-flight facility is a high-intensity neutron source which has been operating at CERN since 2001 [9]. Neutrons are produced by a 20 GeV pulsed proton beam interacting with a solid lead target. The detectors are located about 180 meter downstream. The spectrum predicted by Fluka is the result of a simulation which starts with interacting protons in the

¹The individual results were scaled by $1/(N - 1)$ with N being the respective neutron multiplicity.

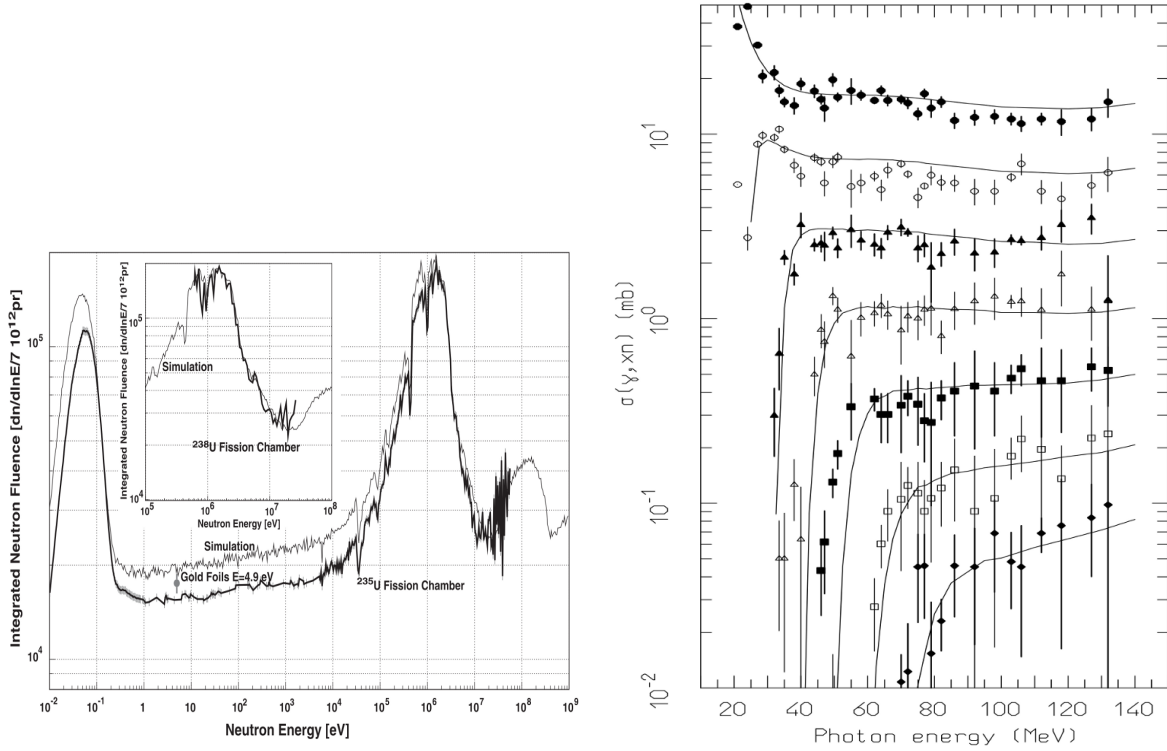


Figure 2: (a) Neutron fluence as a function of energy from measurements with ²³⁵U and ²³⁸U fission chambers. The dashed curve represents the simulated fluence. The value of the fluence at 4.9 eV as determined by the activation of gold foils is also shown. (b) Excitation functions for emission of N or more neutrons from a lead target hit by mono-energetic photons. See text for more details.

lead target and includes the entire experimental geometry with all relevant physics processes.

The agreement between simulated and measured spectrum is apparent, although a 20% discrepancy was found in the energy range from ≈ 0.4 eV to a few MeV. Later, it was noted that a water absorber just downstream of the neutron production target was 1 cm thicker than recorded on the design drawings. When this error was corrected the initial discrepancy in the simulation was removed.

2.3 FLUKA physics options

The physics models in Fluka are fully integrated into the code, so that the user is presented with an optimal approach in the opinion of the developers. Several default settings addressing different general physics problems are available. These can be further modified from the default behavior via Fluka options.

For this study, the simulation was performed with the Fluka default setting PRECISIO(n). In addition, photo-nuclear interactions were enabled through the Fluka option PHOTONUC and a more detailed treatment of nuclear de-excitation was requested with the EVAPORAT(ion) and COALESCE(nce) options. The latter two options are suggested to the user in order to obtain more reliable results for isotope production.

These enable the evaporation of heavy fragments ($A > 1$) and the emission of energetic light-fragments, respectively. The treatment of nucleus-nucleus interactions was also turned on for all energies via the option IONTRANS, and delayed reactions were enabled through the option, RADDECAY.

To evaluate the muon-induced neutron production rate in the simulation, we record neutron captures on hydrogen inside liquid scintillator. This approach closely follows that of the experimental measurement and avoids technical ambiguities for neutron counting.

2.4 Simulation concerning liquid scintillator

As previously noted, all available experimental information about cosmogenic neutrons and muon-induced secondary products are obtained from experiments through the use of liquid scintillator. Depending on the respective detector configuration, the surrounding materials may also significantly contribute to the flux. With respect to Fluka, the following two issues are identified.

2.4.1 Treatment of deuterons in FLUKA

The user can vary the degree of detail for the simulation of nuclear processes in Fluka in order to optimize CPU time constraints and the nature of the physics problem. Because of the focus on neutron and isotope production, a realistic treatment of nuclear de-excitation is mandatory to study cosmogenic neutron production. As a result Fluka produces heavy fragments ($A > 1$) in addition to other particles in the process of returning nuclei to their ground state. In particular for liquid scintillator, a large fraction of the heavy fragments are energetic deuterons. For the simulation of neutron production in liquid scintillator by cosmogenic muons with a mean energy of 283 GeV, the number of neutrons in the final state is reduced by approximately 8% when fragments with $A > 1$ are requested. However, the current version of Fluka implements transport but no interaction model for deuterons. Consequently, all neutrons which are incorporated into deuterons are lost, though some neutrons should be partially recovered through deuteron spallation.

2.4.2 Photoproduction of ^{11}C

In Fluka, nuclear de-excitation is performed according to a Fermi break-up model for light nuclei having mass number $A < 16$. An updated version of this model will be available with the next major Fluka release. The updated model implements additional conservation laws as well as constraints on available final state configurations and symmetries [10]. As a relevant example, the $\gamma + ^{12}\text{C}$ reaction in the current FLUKA model strongly favors break-up of ^{12}C into 3α over neutron emission via photo-production. In this case the parity and spin of the 3α breakup are:

$$\gamma(1^-) + ^{12}\text{C}(0^+) \rightarrow 3\alpha(0^+).$$

Thus even though this is energetically and model favored, the 3α break-up with $L=0$ is forbidden. As a result, the reaction $^{12}\text{C}(\gamma, n)^{11}\text{C}$ is under-predicted by current and previous Fluka versions.

3 Cosmogenic background simulation at LNGS

A faithful simulation of the muon radiation field in the vicinity of any underground experiment requires detailed information of the depth, overburden geometry, and composition of the surrounding rock through which the muons propagate. While the radiation field can be assumed constant at the average depth of the experimental hall, since the cavern size scales are small relative to changes in the flux, details of the detector geometry and materials surrounding the cavern and detector are important.

3.1 Previous FLUKA Simulations

Most all approaches to simulating muon-induced neutron backgrounds in deep underground experiments use a general parameterization of the neutron radiation field in the cavern, as given, for example, in Ref. [11]. The neutron radiation field is created by single muons but other components of the cosmogenic event, and site specific information are not implemented. However, maintaining the complete radiation field significantly modifies the character of the background problem. This can be seen, for example, in the issue involving the $\gamma + {}^{12}\text{C}$ reaction, as pointed out in the previous section.

In an initial study of secondaries induced by muons, we used Fluka to reproduce the muon-induced neutron kinetic energy spectrum for LNGS following the prescriptions given by Ref. [11]. The neutron flux is found for a standardized cubical cavern of dimensions 6 m, permitting single muons to interact in the surrounding 7-m thick layer of rock. The spectra are normalized to the LNGS muon flux of $1.17 \mu\text{hr}/\text{m}^{-2}$ in accordance with measurements. A study of the rock thickness required to equilibrate neutron production is summarized in Figure 3a.

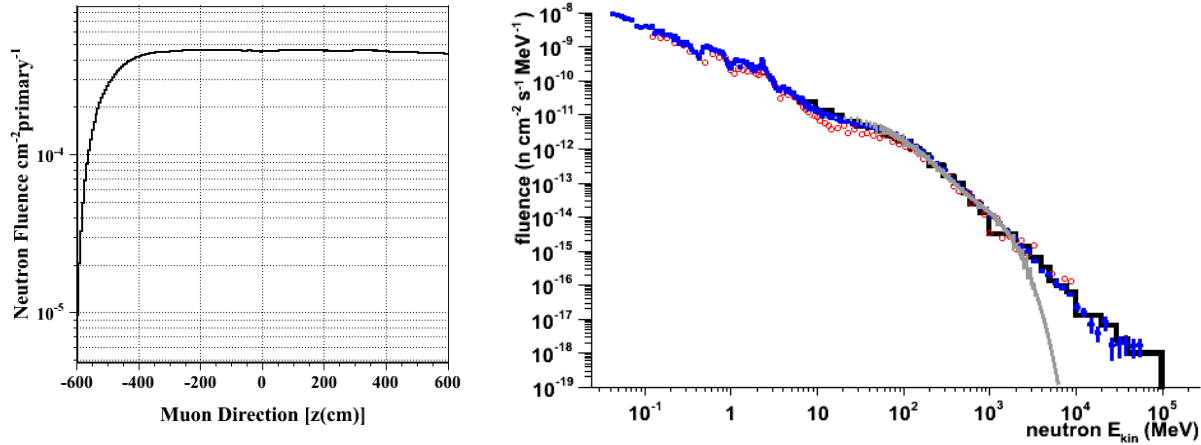


Figure 3: (a) A figure showing the neutron flux as a function of the distance traveled by a muon with 270 GeV kinetic energy [12]. (b) Neutron kinetic energy spectrum as predicted for a cavern at the LNGS laboratory. Blue symbols with statistical errors only: current Fluka, red symbols: Wulandari et al. [13], solid black line: Dementyev et al. [14] and gray line: [11].

Our simulated neutron spectrum is shown in Figure 3b by the solid blue symbols

along with the parameterization given by Ref. [11], indicated by the gray line. Two more predictions from literature are included in this comparison. The open red symbols present a simulation result prepared in the context of the CRESST experiment, also making use of Fluka [13], while the black histogram (for $E_{kin} > 6$ MeV) was derived by the LVD collaboration, in part using the hadronic transport code SHIELD [14]. Both experiments were situated at the LNGS laboratory.

Our standard Fluka results and the predictions for the two experiments are in good agreement over the entire available energy range. In contrast, the distribution and parameterization suggested in Ref. [11] do not reproduce the behavior predicted by FLUKA at high energies. Even though there are few neutrons at these energies, they are of special concern since these energetic neutrons are very penetrating. Further note that all results in Ref. [11] include an independent increase of the neutron multiplicity beyond FLUKA predictions. This correction introduces an extra 30% to the neutron flux and was implemented in Ref. [11] to fit the observed data. However, Figure 3b indicates that other Fluka-based work does not require this additional increase to reproduce the neutron kinetic energy spectrum.

In general, the previous Fluka simulations of deep underground cosmogenic backgrounds do not address several issues to be discussed later, since site and experiment specific information were not included.

3.2 Muon radiation field

3.2.1 Particle components of the muon radiation field

As previously indicated, high energy muons produce many particle types in addition to neutrons. These particles including the primary muon can continue to produce backgrounds as they interact with the detector and its surroundings. Figure 4 shows the particle fluence produced by 250 GeV muons. Aside from neutrons, photo-production can also contribute to backgrounds, including neutron backgrounds due to the large photon flux even though cross sections are due to electromagnetic interactions.

3.2.2 Intensity

The muon flux in the 3 halls at LNGS is summarized in a recent publication [15]. The total muon flux for the simulation described in this paper is normalized to an experimental measurement. More precisely, this measured flux describes the total cosmogenic muon event rate, since individual counts may contain more than one muon [16]. Differences in muon flux between these measurements as given in Table 1 may be attributed to the relative location of the halls within the laboratory, but also could indicate variations due to systematics. For the present simulation, the value given by Borexino was adopted, as this detector is located in Hall C next to the DarkSide experiment.

3.2.3 Mean energy and differential energy spectrum

The underground muon kinetic energy spectrum can be approximated by the following relation [17]:

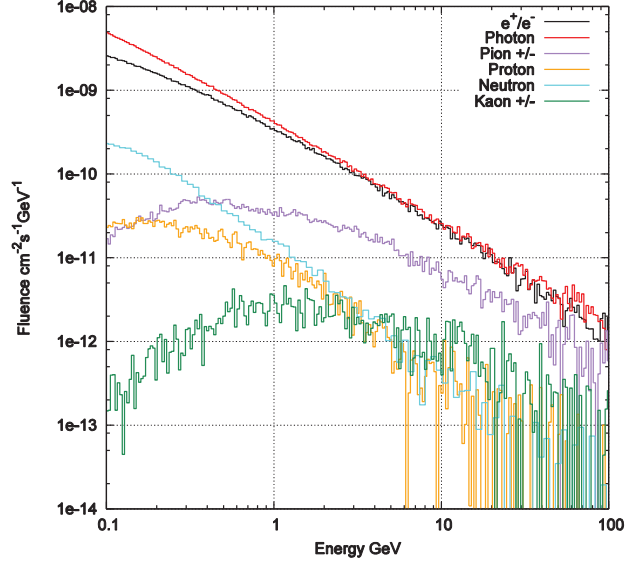


Figure 4: Particle fluence produced by 250 GeV muons on rock

Table 1: The table shows the measured muon flux in the various experimental halls at the LNGS

experiment	Hall	year published	total muon event rate ($\times 10^{-4} \text{ s}^{-1} \text{ m}^{-2}$)
LVD	A	2009	3.31 ± 0.03
MACRO	B	2002	3.22 ± 0.08
Borexino	C	2012	3.41 ± 0.01

$$\frac{dN}{dE_\mu} = \text{const} \cdot (E_\mu + \epsilon(1 - e^{-\beta h}))^{-\alpha}$$

In the above, E_μ is the muon kinetic energy at slant depth h , and α is the surface muon spectral index. For this approximation the quantities β and ϵ are related to muon energy loss mechanisms in rock, and are assumed constant. From the above equation, the average muon kinetic energy at slant depth h is:

$$\langle E_\mu \rangle = \frac{\epsilon(1 - e^{-\beta h})}{\alpha - 2}$$

Experimental results for the spectral index α and the mean muon energy for LNGS were reported by MACRO [17] and are reproduced in Table 2:

Table 2: The mean energy of single and double muon events as measured by MACRO

event type	mean muon energy (GeV)	spectral index α
single muon	$270 \pm 3_{(stat)} \pm 18_{(syst)}$	$3.79 \pm 0.02_{(stat)} \pm 0.11_{(syst)}$
double muon	$381 \pm 13_{(stat)} \pm 21_{(syst)}$	$3.25 \pm 0.06_{(stat)} \pm 0.07_{(syst)}$

The functional description of the energy spectrum given by equation (3.2.3) permits direct sampling since it can be integrated and inverted in analytic form. Adopting the values $\epsilon = 0.392 \times 10^{-3}$ and $\beta = 635$ GeV this procedure reproduces the measured mean energy for single and double muon events, and gives an overall mean energy of 283 ± 19 GeV for cosmogenic muons at LNGS.

3.2.4 Bundles

Muon bundles were investigated at LNGS by the LVD and MACRO experiments. The experimental results used here were taken from MACRO [18]. Figure 5 shows the measured muon multiplicity and the spatial separation between muons for double muon events. A simulation to study muon multiplicity used simplified sampling of the distribution up to a muon multiplicity of 4. The distance between muons within a bundle was chosen according to the distribution measured for double muon events, and all muons within a bundle are given the same direction.

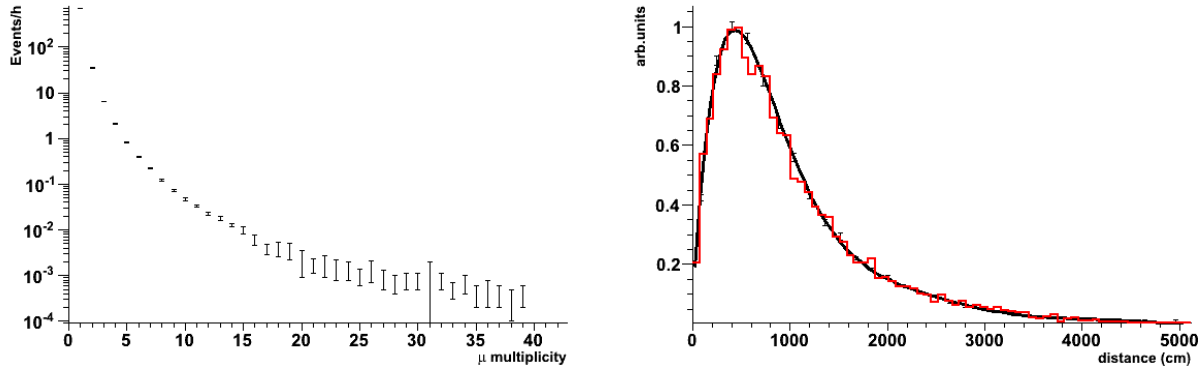


Figure 5: (a) Multiplicity of muons recorded by the MACRO detector for cosmogenic muon events. (b) Spatial separation of muons obtained for cosmogenic events in the MACRO detector featuring two coincident muons (red data points). The black line shows a simple higher order polynomial fit used to implement sampling of the distribution.

The effect of multi-muon events for the Borexino detector geometry was evaluated assuming the measured multi-muon event rate of about 6% from MACRO. Approximately 1.5% of muon events in Borexino feature more than one muon. In addition, about 12% of the single muons crossing the Borexino inner detector belong to multi-muon events.

3.2.5 Event generation

In order to implement the simulation, a combination of azimuthal and zenith angles is selected according to the measured muon angular distribution. A map of the LNGS (Gran Sasso mountain) overburden, which was prepared by the MACRO collaboration [19, 20], is used to translate the muon direction into the respective slant depth h . Next, the muon event type is set to either a single muon or muon bundle event. In the case of muon bundles, a multiplicity of up to 4 muons is sampled from the measured

multiplicity spectrum. The probability for muon events with larger multiplicity is less than 0.2% and these events are treated as muon bundles of multiplicity 4 to simplify the calculation.

Finally, the muon kinetic energy is selected as a function of slant depth h and muon event type by sampling from the parameterized single or double muon event spectrum. The latter is used for muon bundle events of all multiplicities since no experimental information is available for events with higher muon multiplicities. About 1.4% of the cosmogenic events at LNGS contain more than 2 muons.

The muon events are randomly placed on a plane located above the hall geometry. A sufficiently large plane above the hall is considered to fully illuminate the hall including the detector. Other muon tracks outside this envelope are rejected.

3.2.6 Angular distribution

The slant depth of the muon transit through the rock overburden depends on both azimuthal and zenith angles. The azimuthal angular dependence of the slant depth in rock, h ($g\,cm^{-2}$), depends on the profile of the Gran Sasso mountain covering the experimental cavern. Hence, both the intensity and energy profiles of the muons are a function of their incident direction on the detector.

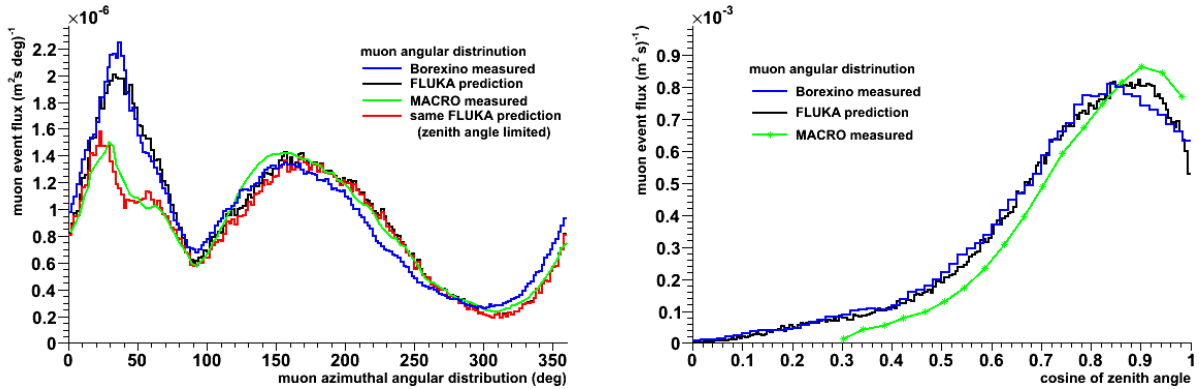


Figure 6: Muon azimuthal (a) and zenith (b) angular distribution at LNGS for polar coordinate system pointing up and North with clockwise increasing angle. Blue line: Borexino data, green line: MACRO data, black (red) line: Fluka predictions (zenith angle limited).

A measurement of the cosmogenic muon angular distribution at LNGS was performed by MACRO [21] for Hall B. Azimuthal and zenith projections of the distribution are shown by the green histograms in Figure 6. The distributions are compared to recent results from Borexino [22] for Hall C given by the blue histograms. The difference in the experimental azimuthal spectra for angles near 45 degrees is caused by the MACRO zenith angular acceptance limit of about 60 degree. The data are compared to a Fluka simulation which traced muons, initiated by cosmic rays in the upper atmosphere, to the experimental halls [20]. The spectra were normalized to the Borexino measured total muon flux. The predictions for full detector acceptance are shown by the black histograms in Figure 6. Imposing the zenith angle limitation of MACRO in the simulation reproduces the same feature as found in the data. The resulting azimuthal

spectrum is shown by the red histogram. Good agreement is found between data and predictions. The small visible shift in the azimuthal distribution is due to the change of location for the two experiments.

3.3 Muon-induced secondaries

3.3.1 Geometry

The cosmogenic radiation field at deep underground sites is composed of muons and muon-induced secondaries. Incident muons are allowed to develop particle showers as they pass through a 700 cm thick layer of Gran Sasso rock [19] surrounding all sides of Hall C. The rock thickness to fully develop the shower was determined by simulation, see Figure 3a. However for computational purposes, this thickness was divided into three sections to permit simulation of electromagnetic processes with increasing detail as the shower approached the cavern. The basic assumption of this procedure is to implement an initially homogeneous distribution of muons at every space point within the rock of appropriate direction and energy.

3.3.2 Propagation through rock

The cosmogenic radiation which is present at the cavern walls is approximated in two separate steps to reduce computation time. In the first step, the muon radiation field as described in the previous section, is considered. These muons were located on the outside of the rock layer surrounding Hall C, and allowed to propagate without interactions through the rock and recorded if they entered the hall. At these high energies, the muon trajectory is approximately unchanged by interactions. Muons entering the hall were then propagated a second time with all physics processes enabled to derive a description of the cosmogenic radiation field including all muon-induced secondaries. All secondaries are treated as part of the event.

3.3.3 Connection of simulation to measured muon event flux

The muon flux, Φ_{sim} , inside the cavern expressed per simulated muon event, is determined by the simulation as described above. An empty spherical volume was inserted inside the cavern, and exposed to the muon radiation field in order to determine the flux incident on the Borexino detector. The muon fluence estimated by the track length-density inside the sphere was obtained by a standard Fluka scoring option. Choosing a spherical volume to obtain the muon fluence correctly accounts for the angular distribution of the muons. Moreover, the fluence through a sphere is a direct estimator for the flux through the cross sectional area of the sphere.

The length of the time-period considered in the simulation (lifetime), is given by the number of simulated muon events compared to the ratio of the simulated to measured total muon flux, Φ_{exp} , from Table 1.

$$T[s] = N_{events} \cdot \frac{\Phi_{sim}[events^{-1}cm^{-2}]}{\Phi_{exp}[s^{-1}cm^{-2}]}$$

4 Validation

The Fluka predictions using Borexino as a model, are now compared to available data from similar experiments at comparable depth with a focus on the more recent measurements. These include a new analysis from the LVD experiment [23, 24] located in Hall A at LNGS and results available from the KamLAND detector [25] which is operated at the Kamioka mine at a similar depth.

Available information about muon-induced secondaries deep underground is limited to measurements of cosmogenic neutrons and isotopes in large liquid scintillator detectors. As an example, a realistic model of the Borexino experiment [26, 27] was implemented in Fluka in order to validate a FLUKA simulation of neutron production. The Borexino detector features a well shielded, large volume liquid scintillator and provides high quality measurements of cosmogenic muon-induced neutrons with reduced systematic uncertainties in addition to the available results for the cosmogenic muon flux and the ^{11}C production rate.

4.1 Detector geometries

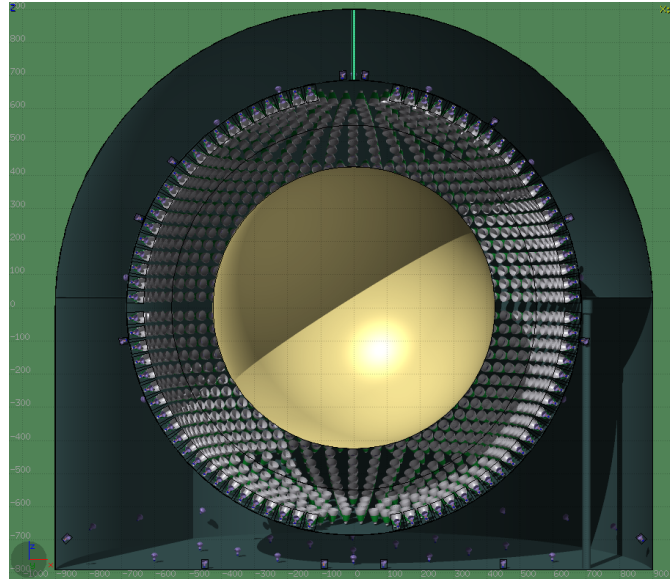


Figure 7: A view of the Fluka implemented Borexino detector geometry. The sensitive volume of the Borexino detector, the Inner Vessel, is shown by the golden sphere. It is centered inside two (transparent) buffer regions which are contained inside a stainless steel sphere which supports the optical modules. This inner detector is placed inside a domed, cylindrical water tank which functions as a Čerenkov detector to identify and help track cosmogenic muons.

A cross-sectional view of the geometry implemented for the Borexino experiment is given in Figure 7. The central sensitive liquid scintillator region of radius 425 cm having a mass of approximately 278 tons is contained in a spherical, nylon inner vessel. It is located at the center of a 685 cm radius Stainless Steel Sphere (SSS) filled with inert liquid scintillator as a passive shield. The SSS in turn is placed inside a 900 cm radius

domed, cylindrical water tank providing additional shielding which functions as a water Čerenkov muon veto detector. The material of the detector components are carefully modeled in the simulation according to available information for Borexino. The liquid scintillator is Pseudocumene with the addition of a 1.5 g/l fraction of wavelength shifter 2,5-diphenyl-oxazole ($C_{15}H_{11}NO$). The Fluka simulation also implemented the photo-sensors of the inner detector, but no attempt was made to include optical transport and detector effects or to address the creation of realistic detector signals. Instead, the production of cosmogenic isotopes as well as neutron capture reactions on hydrogen inside the Inner Vessel were recorded.

Available data on muon-induced neutrons in underground laboratories before 2007 was summarized in Ref. [28]. It should be pointed out that this report includes most of the available data and that these data were obtained with similar systematic uncertainties. In addition to the data, more recent results from the LVD experiment are available. These new results are based on an analysis making use of a detailed simulation of the full LVD detector [23]. The new results differ significantly from earlier published values for the same experiment. Further, experimental data is now available from the KamLAND experiment. The KamLAND detector is very similar in design to Borexino and situated at a comparable depth. It has a reported average muon energy of 260 ± 8 GeV [25].

Both measured and Fluka simulated results are presented for the neutron yield and cosmogenic isotope production. A measurement of the ^{11}C production in liquid scintillator was also recently published by the Borexino experiment [29]. All experimental information is based on neutron capture measurements in liquid scintillator detectors.

4.1.1 Total muon-induced neutron yield

The most measured quantity for studying cosmogenic backgrounds is the total muon-induced neutron yield in liquid scintillator. Figure 8 gives a summary of the reported neutron yield as a function of mean muon energy. The early measurements described in Ref. [28] are shown by the solid black symbols together with a prediction (black line) which predates most measurements. Two values are given for the LVD experiment which differ by more than a factor of 2. The earlier lower yield was later explained by an additional energy threshold on the cosmogenic neutrons [30].

The two LVD results were followed by a new analysis making use of a full detector simulation shown by the solid green symbol². Another measurement of the neutron yield at LNGS was reported by the Borexino collaboration (solid red symbol) just before the first LVD result was made public. The detector volume was rather small and only single cosmogenic neutrons per crossing muon could be recorded due to the data acquisition system [32].

The neutron yield as measured by the KamLAND experiment is shown by the solid blue symbol. It is compared to the reported Fluka predictions given by the open blue symbol. However, the simulated neutron yield can be corrected *a posteriori* for the incorrectly simulated rate of ^{11}C production as will be shown in the next subsection. This correction increases the predicted neutron yield which is also indicated in Figure 8.

²The evolution of the LVD result for the cosmogenic neutron yield is indicative of the challenges to perform this measurement. The assigned systematic experimental uncertainties should be considered somewhat optimistic for older data points.

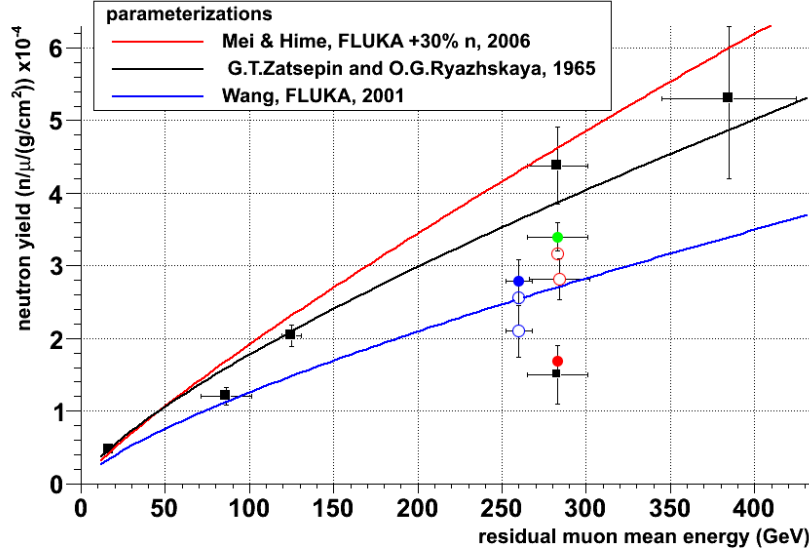


Figure 8: Comparison between experimental data and simulation for muon-induced neutron yield in liquid scintillator as a function of mean muon energy: from report [28] (black), most recent LVD (solid green), KamLAND (solid blue) and CTF (solid red). The open circles are Fluka predictions, see text for details. Different suggested parameterizations of the neutron yield are shown by the thin lines: from report [28] (black), Mei and Hime [11] (red) and Wang [31] (blue).

Note that the Fluka results for KamLAND were obtained with a simplified muon-induced radiation field and detector description. Additionally, the reduced neutron count resulting from the missing deuteron interaction model in Fluka and possible subsequent spallation were not addressed.

The open red symbols are the preliminary results for the neutron yield obtained from the current Fluka simulation. The neutron yield after applying the same *a posteriori* correction is also indicated. The Fluka predicted neutron yield in liquid scintillator material at energies close to the mean muon energy for LNGS of 283 ± 19 GeV is in good agreement with more recent experimental data. Also shown in the Figure 8 are two previously suggested parameterizations derived by using Fluka. The blue curve was given by Wang [31] while the red curve is taken from the work of Mei and Hime [11] which used an extra 30% renormalization of the cosmogenic neutrons.

4.1.2 Cosmogenic isotope production

Radioactive isotopes produced by cosmic radiation are an important background to low-energy solar neutrino spectroscopy experiments like KamLAND and Borexino. Of the produced radioactive isotopes, ^{11}C poses the largest challenge because of its relatively long mean lifetime of approximately 30 minutes. Therefore, the ^{11}C production rate was studied extensively. The current situation is depicted in Figure 9 as a function of time.

As can be seen, the Fluka predicted ^{11}C production rate agrees with early measured results. However, newer and more reliable measurements indicate a production rate about twice as large. Because of missing details when simulating the Fermi-breakup of

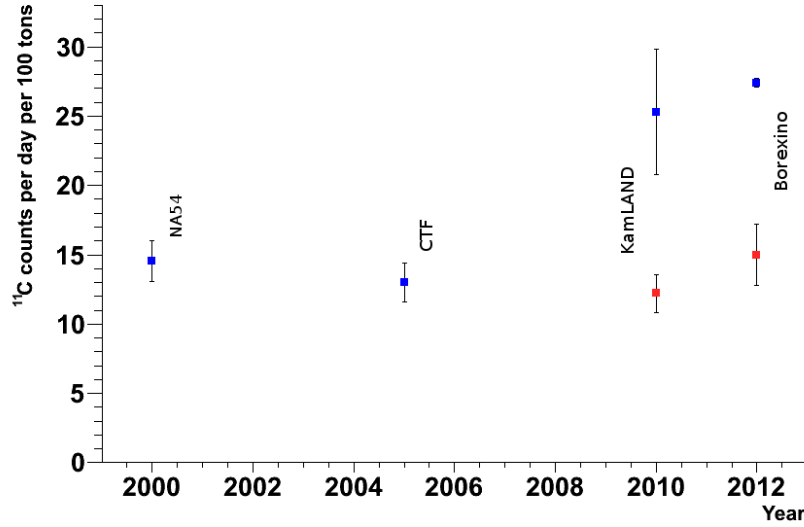


Figure 9: Cosmogenic ^{11}C production per day for the nominal 100 ton fiducial volume of the Borexino detector. Rates derived by scaling from earlier available experimental data (CERN experiment NA54 [33] and CTF [34]) are compared to the recently published ^{11}C production rate (solid blue symbols) measured by KamLAND and Borexino. Error bars show the reported experimental uncertainties. Also shown are Fluka predictions for the ^{11}C production rate (solid red symbols) from KamLAND and the current simulation.

^{12}C in the current version of Fluka, see subsection 2.4.2, a significant underproduction of ^{11}C is now expected.

The measured production yield reported by KamLAND for ^{11}C of $0.866 \pm 0.153 \times 10^{-4} (\mu\text{g}/\text{cm}^2)^{-1}$ is about 1/3 of the neutron production yield of $2.787 \pm 0.311 \times 10^{-4} (\mu\text{g}/\text{cm}^2)^{-1}$. Further, KamLAND confirmed that about 96% of the production of ^{11}C proceeds through the photoproduction reaction $^{12}\text{C}(\gamma, n)^{11}\text{C}$ which produces a neutron. Consequently, the under-prediction of ^{11}C production by Fluka, results in a reduced neutron yield. Simple *a posteriori* scaling permits a cursory correction of the Fluka predictions for the neutron yield based on the measured and simulated ^{11}C production rates for the KamLAND and Borexino simulations.

The under-predicted rate of ^{11}C production for liquid scintillator material is responsible for a large fraction of the reported problems with the number of cosmogenic neutrons predicted by Fluka. It is important to recognize the source of this missing component. The class of missing neutrons from the simulation are not high energy neutrons as they are produced by photo-nuclear interactions from the significant flux of real photons in the muon radiation field.

4.1.3 Distance between neutron capture and muon track

The lateral distance distribution of the neutron capture location from the parent muon track is shown in Figure 10a. The thin blue histogram reflects the Fluka prediction of the distribution for the Borexino detector. The shape and extent of the distribution is biased by the geometry and size of the detector. The thick black histogram

is obtained by folding the simulated distribution with the muon track reconstruction uncertainties [26]. In addition, both the distance of the muon track and the neutron capture point from the detector center were restricted to less than 400 cm. The effect of the muon track uncertainties is most visible for neutron captures close to the parent muon track while the restriction in distance from the detector center impacts the shape and extent of the distribution.

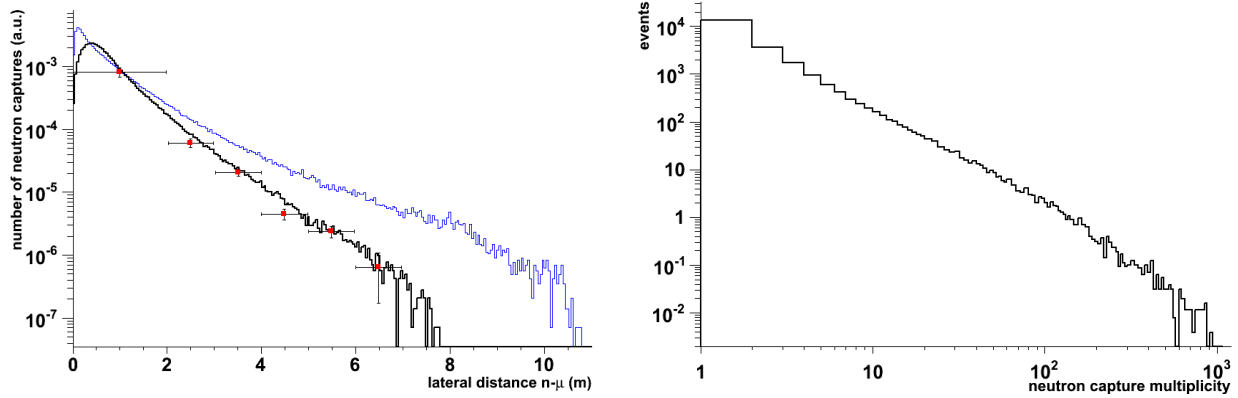


Figure 10: (a) Comparison between experimental data (solid blue symbols) from LVD [35] and Fluka predictions (black histogram) for the distance between neutron capture and the muon track. (b) Muon-induced cosmogenic neutron multiplicity as predicted by Fluka. Events with neutron multiplicities of several hundreds of neutrons per event are expected.

The shape of the predicted distribution is compared to available data from the LVD experiment [35] (solid red symbols). The experimental distribution is well reproduced by the simulation when the effective size of the Borexino detector is limited to a radius of 400 cm.

4.1.4 Neutron multiplicity

Figure 10b presents the cosmogenic neutron multiplicity distribution as predicted by FLUKA for the Borexino detector. Some events with very large multiplicities are found. No experimental spectrum for the cosmogenic neutron multiplicity distribution is available. A measurement of the neutron multiplicity is expected from the Borexino experiment in the near future.

5 Cosmogenic background predictions for DarkSide

The DarkSide detector will be installed inside the Counting Test Facility (CTF) which is located in Hall C at LNGS adjacent to the Borexino detector. Because of the proximity of the two experiments, the same muon induced cosmogenic radiation field which was used for the comparison to available experimental data can also be used to simulate the cosmogenic background for DarkSide.

5.1 Detector geometry

The DarkSide detector consists of a cylindrical, two-phase underground liquid argon Time Projection Chamber (TPC) [36]. The TPC is contained inside a thin-walled stainless steel Dewar. The sensitive region is viewed by photomultiplier tubes from the top and bottom. It is surrounded by a TPB coated Teflon cylinder which acts as an optical reflector and wavelength shifter. The Teflon cylinder also supports a set of copper rings which provide the electric field. The DarkSide-50 experiment with an active mass of 50 kg is currently under construction. It features a sensitive volume of about 35 cm diameter and 35 cm height. The inner detector will be immersed in a highly efficient, borated Liquid-Scintillator neutron Veto (LSV) to reduce external backgrounds and to monitor cosmogenic and radiogenic neutron backgrounds *in situ*. To further reduce cosmogenic backgrounds, the LSV is surrounded by ultra pure water inside a large cylindrical water tank (CTF) which functions as muon veto Čerenkov detector. The CTF will also provide a passive shield against low energy external backgrounds. The implementation of DarkSide in FLUKA is shown in Figure 11.

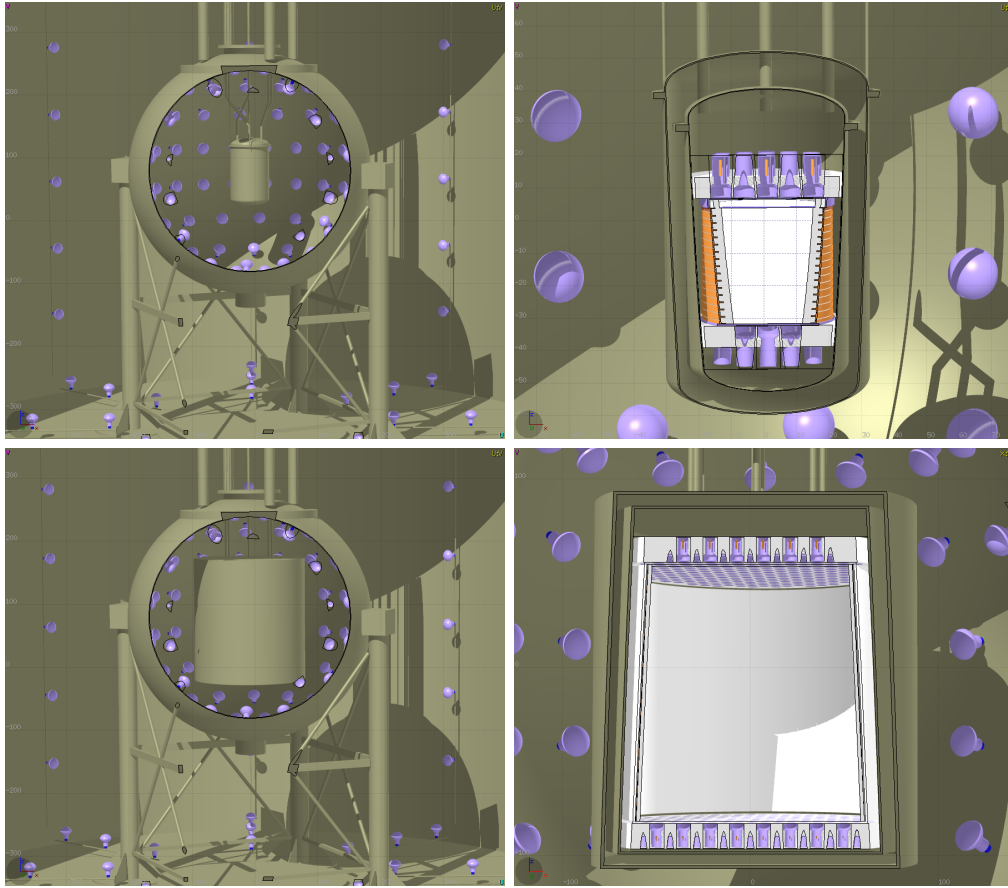


Figure 11: Fluka implementation of the DarkSide experiment. The Dewar containing the TPC is shown mounted inside the LSV on the left while the graphs on the right expose details of the geometry implemented for the TPC. Top row: DarkSide-50; Bottom row: DarkSide-G2.

The DarkSide experiment is in addition to its scientific reach, also a prototype for

the development of a ton-sized, next generation TPC, as the design of the veto detector system permits the upgrade to DarkSide-G2 with a sensitive mass of approximately 3.3 tons of underground liquid argon. The ton-sized TPC features a sensitive volume of about 150 cm diameter and 135 cm height. In general, the rate of cosmogenic neutron background scales with the size of the sensitive detector volume and is substantially larger for DarkSide-G2 compared to that of DarkSide-50. Similarly, the increased size of the TPC displaces a larger amount of liquid scintillator inside the LSV and reduces the efficiency of detecting neutrons.

5.1.1 Counting Test Facility

The CTF [37] is modeled in this simulation as a cylindrical tank of 11 meter diameter and 10 meter height constructed from 8 mm thick carbon steel. It is filled with ultra pure water and placed on an additional 10 cm thick layer of steel. The inside tank surfaces are covered by sheets of a special type of layered Tyvek foil [38] to enhance light collection. For the relevant spectral range determined by the produced Čerenkov light and the sensitivity of the PMTs, a reflectivity in water of greater than 95% is expected. In the simulation a more conservative constant reflectivity of 80% was assumed. Čerenkov light produced in the water is measured by 80 ETL-9351 eight-inch PMTs which are placed along the floor and the walls of the CTF. The production, propagation and detection of the Čerenkov photons in the CTF is simulated in detail by FLUKA taking into account a constant refractive index of 1.334 and a realistic absorption spectrum for pure water [39]. The photo sensors are modeled with their measured quantum efficiency spectrum scaled by a 70% photoelectron collection efficiency [40]. A study to evaluate the placement of the PMTs indicated only a weak dependence of the overall efficiency to detect muons as a function of the spatial distribution of the optical sensors. The insensitivity to the spatial dependence is attributed to the low absorption in pure water combined with the high surface reflectivity.

5.1.2 Liquid-Scintillator neutron Veto

The LSV [41] is implemented as a 4 meter diameter stainless steel sphere with 8 mm wall thickness. It is filled with a borated liquid scintillator consisting of a 1:1 mixture of Pseudocumene and Trimethylborate. The sphere is located inside the CTF and both the inside and the outside surfaces are covered by the Tyvek reflector. The LSV is equipped with 110 low-background glass-bulb Hamamatsu R5912-HQE-LRI eight-inch PMTs which are mounted on the sphere facing inward. Optical processes inside the LSV were not simulated. Instead, the un-quenched raw energy deposition per event is recorded.

5.1.3 Inner detector

Both, the DarkSide-50 and the DarkSide-G2 [36, 42] configurations of the inner detector were implemented in the FLUKA simulation. Initial studies were carried out for the smaller DarkSide-50 design, however the following results are for the ton-sized DarkSide-G2 geometry. In this case, the cosmogenic background requirements are more stringent as DarkSide-G2 has a much larger sensitive volume. Thus the results

can be viewed as a conservative upper limit to those expected for DarkSide-50. The geometry and material composition of the Dewar and TPC for the DarkSide-50 setup were modeled in detail according to the latest detector design drawings. This was then used to prepare a realistic, scaled model for the ton-sized configuration. In the simulation the sensitive volume is viewed by 283 three-inch Hamamatsu, low-background R11065 PMTs positioned on the top and an equal number on the bottom of the TPC. As for the LSV, no simulation of the optical processes inside the TPC were undertaken. The number of particles entering the sensitive volume, their type and the total raw energy deposited per event were recorded.

5.2 Simulation results

Starting from full cosmogenic events which were “frozen” on the walls inside of the experimental Hall C at LNGS, all particles were transported by FLUKA through the section of the cavern which contains the DarkSide-G2 experiment. Results are presented based on a total number of simulated cosmogenic events corresponding to a lifetime of approximately 36 years. The statistical uncertainty of the results is of the order of a few percent, and in any event, is smaller than the systematic uncertainties. Events for which at least one particle reached the CTF water tank were recorded as a first step. The predicted rate for these cosmogenic events at the outside of the CTF is approximately 3.45 events per minute. For about 23% of the events, the original cosmogenic muon does not reach the CTF water tank.

The complete DarkSide-G2 detector setup was then exposed to all events which were recorded at the outside of the CTF in a second step of the simulation. All physics processes were turned on making use of the FLUKA defaults setting PRECISIO(n). In this step of the simulation Čerenkov photons were created inside the CTF water tank. However, because of CPU considerations they were not initially transported. The rate of cosmogenic events with at least one particle reaching the LSV is predicted to be approximately 0.30 events per minute. This reduction in rate is the result of both the smaller size of the volume and the passive shielding of the water tank. Similarly, the rate of cosmogenic events with at least one particle reaching the sensitive region inside the TPC is predicted by FLUKA to be 0.07 events per minute. The decrease in rate is caused by the smaller size of the sensitive liquid argon region and the passive shielding of the liquid-scintillator. Reported rates are upper limits since no energy deposition in the respective detectors was required. The expected cosmogenic event rates are summarized in Table 3.

Table 3: Expected cosmogenic event rates	
just outside of	cosmogenic event rate (per minute)
CTF	3.45
LSV	0.30
sensitive liquid argon region	0.07

In order to further study the predicted cosmogenic background to the DarkSide-G2 experiment the subset of events with at least one particle reaching the inner sensitive region was considered. Events with more than 50 coincident particles reaching the

sensitive volume were also rejected since these give a clear signal in the TPC and can be rejected. When these cuts are applied, the fraction of cosmogenic events in which the original muon does not enter the CTF is reduced to 7.7 events per year.

In Figure 12 the raw energy deposited inside the CTF and the LSV are graphed with respect to each other. Cosmogenic events with at least one particle reaching the sensitive liquid argon volume almost always deposits a significant amount of energy inside the veto detectors. The dominant region in the scatter plot is indicated by the red box and limited by $dE_{(CTF)} > 1.3$ GeV and $dE_{(LSV)} > 0.2$ GeV. This region corresponds

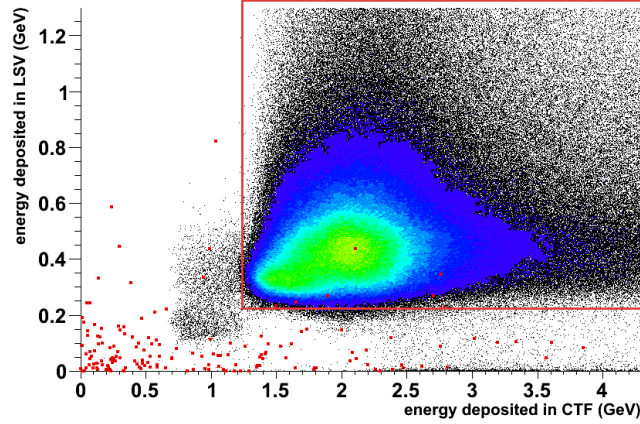


Figure 12: Energy deposition inside CTF and LSV for cosmogenic events with at least one particle reaching the sensitive volume of the inner detector.

to events with the original cosmogenic muon traversing both detectors. The superimposed color contour plot indicates the shape of the most frequent energy deposition for cosmogenic events resulting from the ionization of the relativistic muons. Events with similar energy deposited inside the CTF but with $dE_{(LSV)} < 0.2$ GeV indicate that the original muon traversed the CTF but missed the LSV. A smaller set of events in the region of $0.7 \text{ GeV} < dE_{(CTF)} < 1.3$ GeV results from low energy cosmogenic muons which traverse the water tank but stop inside the LSV. The most difficult cosmogenic events to veto are found close to the origin of the graph. For these events, little energy is deposited both inside the CTF and the LSV. Cosmogenic events predicted by FLUKA without a direct muon into the CTF are superimposed on the graph with solid red symbols. Practically all cosmogenic events which have small energy deposition in both the CTF and LSV fall into a class of events with no direct muon entering the CTF.

The most important background events for the direct dark matter search consist of neutron-induced recoils in the sensitive volume from undetected neutrons. In the next step of the simulation, all events for which at least one neutron (but < 50 coincident particles) reached the sensitive liquid argon region were reprocessed with full treatment of optical processes inside the CTF. A total of 19735 of these events, or 581 events per year, are predicted by FLUKA. Only the raw energy deposited inside the LSV and the sensitive region of the TPC are available in the current simulation. Therefore, conservative criteria were defined to select events which are considered detectable by the LSV: $dE_{(LSV)} > 1$ MeV, and for events which fall into the energy range of a possible dark matter signal in the TPC: $0 < dE_{(TPC)} < 1$ MeV [42].

The predicted response of the veto detectors is shown in Figure 13 for an equivalent

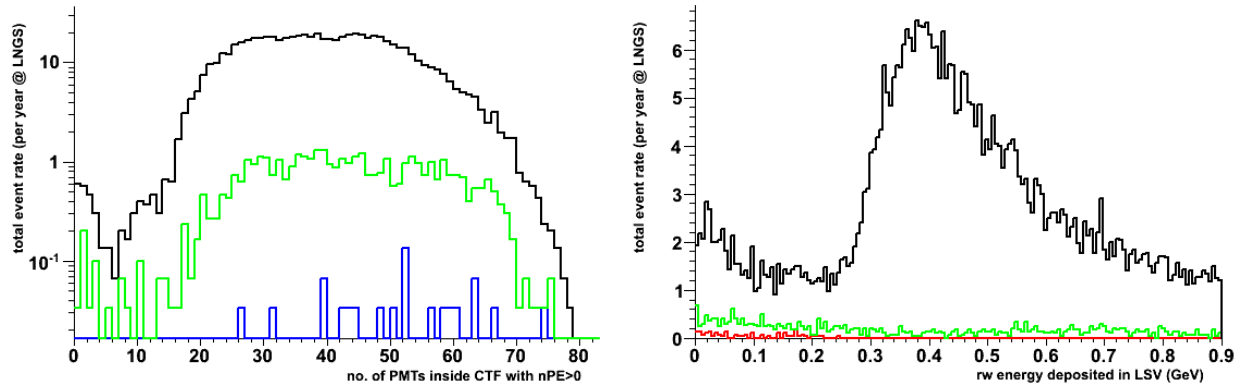


Figure 13: (a) Number of PMTs with at least 1 registered photoelectron. black: all events, green: raw dE inside TPC > 0 and < 1 MeV, and blue: raw dE inside the LSV < 1 MeV. (b) Un-quenched energy deposited inside the LSV. black: all events, green: raw dE inside TPC > 0 and < 1 MeV, and red: < 10 PMTs with at least 1 registered photoelectron.

lifetime of approximately 36 years at LNGS. The number of events found for the CTF as a function of PMTs which register a signal (one or more photoelectrons) is given by the black histogram on the left. The events shown by the blue histogram are found if the energy deposited inside the LSV is limited to less than 1 MeV. The black histogram in the graph on the right shows the predicted energy spectrum for the LSV. Limiting the sample to events with less than 10 PMTs registering a signal inside the CTF reduces the energy spectrum to the events shown by the red histogram. The effect of selecting events in the energy range of interest for the TPC is shown for both distributions by the green histograms.

The same information with focus on events with energy less than 14 MeV deposited in the LSV are shown in Figure 14. The number of PMTs with a signal inside the CTF is graphed versus the raw energy deposited in the LSV. Ten events with less than 3 PMTs recording a signal inside the CTF are considered to be missed by the muon veto and are colored red in the plot. Similarly, twenty-one events with a raw energy deposition of less than 1 MeV inside the LSV are considered missed and are colored blue in the graph.

The FLUKA simulation predicts approximately 581 events per year in which at least one cosmogenic muon-induced neutron enters the sensitive liquid argon volume. Out of these events, only 0.3 events per year fail to cause a signal in 3 or more PMTs of the CTF muon Čerenkov veto. At the same time, only 0.6 events per year deposit less than 1 MeV inside the LSV. For a simulated live-time of approximately 36 years at LNGS, no event occurs where a neutron reached the sensitive liquid argon region but failed to trigger at least one of the two veto detectors. The rates reported are obtained without considering information from the TPC to further reject cosmogenic neutron events.

The cosmogenic muon-induced neutron background rate to the DarkSide-50 experiment is significantly smaller than for the much larger DarkSide-G2 configuration, while the same veto detectors are used for both implementations. The rejection of external cosmogenic neutrons by the LSV increases for DarkSide-50 since there is more liquid-scintillator volume. In addition, this also increases the amount of passive shielding.

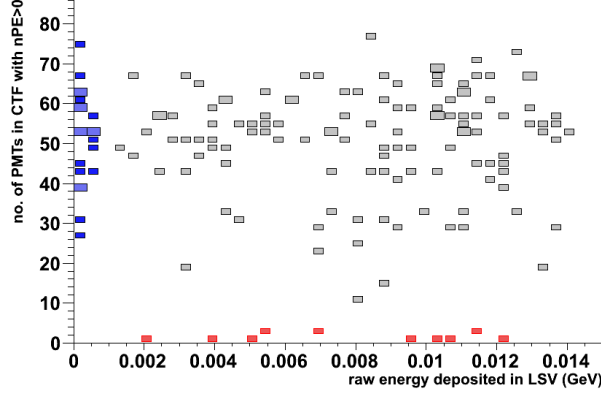


Figure 14: Shown is the of number of PMTs which registered at least one photoelectron inside the CTF versus the un-quenched energy deposited in the LSV. The red and blue color coded entries correspond to the respective events selected in Figure 11.

6 Conclusions

FLUKA predictions for cosmogenic muon-induced neutron backgrounds are found to be in reasonable agreement with available data. A few additional problems were identified and will be resolved in future versions of the code. Corrections relating to the (γ, n) cross section on ^{12}C for example, can be approximately included in the final results, as was discussed in the paper. However, the discrepancy and suggested correction reported in Ref. [11] were found invalid.

The need of a detailed description of the full muon-induced radiation field for the considered underground site was described and shown to be important. Steps to explicitly prepare the cosmogenic radiation field with the FLUKA simulation package were described and the muon-induced radiation field which was used to carry out benchmark studies, was then applied to the DarkSide experiment. Background predictions for a direct dark matter search experiment were obtained for the next generation, ton-sized two-phase underground liquid argon detector. It was found that the proposed dual active-veto system for the experiment provides sufficient shielding against cosmic radiation at the LGNS depth for a ton-sized DarkSide-G2 experiment for more than 5 years.

Background levels for the DarkSide-50 experiment, which use the same veto detector system, are expected to be significantly reduced because of the smaller size and the consequently increased volume of the liquid-scintillator shield and thus adequate for the smaller detector. In the future it is essential to monitor the cosmogenic neutron background levels, with focus on the veto detector system, in order to continue to benchmark the simulation. Work is ongoing to extend the FLUKA studies to new, quality data on cosmogenic neutrons which will be available from the Borexino experiment.

Acknowledgements

This work was supported in part by NSF awards 1004051 and 1242471. We would like to thank Alfredo Ferrari and Maximillian Sioli for FLUKA related help and acknowledge the use of FLAIR. We also would like to thank David D'Angelo, Quirin Maindl and Michael Wurm of the Borexino collaboration.

References

- [1] V. S. Narasimham. Perspectives of experimental neutrino physics in India. *Proc Indian Natn Sci Acad*, 70(A1):11–25, January 2004.
- [2] G. Battistoni, S. Muraro, P.R. Sala, F. Cerutti, A. Ferrari, S. Roesler, A. Fassò, and J. Ranft. The FLUKA code: Description and benchmarking. *AIP Conference Proceeding*, 896:31–49, 2007.
- [3] A. Fassò, A. Ferrari, J. Ranft, and P.R. Sala. FLUKA: a multi-particle transport code. 2005.
- [4] FLUKA Collaboration. FLUKA manual, ASCII or .pdf file available from FLUKA website and contained in FLUKA package, November 2011.
- [5] FLUKA Collaboration. FLUKA official website, <http://www.fluka.org>, 2012.
- [6] A. Antonelli, G. Battistonii, A. Ferrari, and P. R. Sala. Study of radiative muon interactions at 300 GeV. *Frascati Physics Series, Calor 96*, VI:561–570, 1997.
- [7] A. Fassò, A. Ferrari, and P. R. Sala. Designing Electron Accelerator Shielding with FLUKA. *Proc. 8th Int. Conf. on Radiation Shielding*, pages 643–649, April 1994.
- [8] C. Borcea et al. Results from the commissioning of the n_TOF spallation neutron source at CERN. *Nucl. Instrum. Meth. A*, 513:524–537, 2003.
- [9] nToF collaboration. TOF: Proposal for a neutron time of flight facility. *CERN-SPSC-99-8*, 1999.
- [10] the FLUKA collaboration P. Sala et at. New Developments in FLUKA. *CERN Conference Proceeding, Varenna - 13th International Conference on Nuclear Reactions - FLUKA*, June 2012.
- [11] D.-M. Mei and A. Hime. Muon-induced background study for underground laboratories. *Phys. Rev. D*, 73(5):053004, Mar 2006.
- [12] R. J. Jasim. *Monte Carlo Evaluation of Cosmogenic neutron background at Gran Sasso*. PhD thesis, University of Houston, 2011.
- [13] H. Wulandari, J. Jochum, W. Rau, and F. von Feilitzsch. Neutron background studies for the CRESST dark matter experiment. *arXiv HEP-EX/0401032*, 2004.
- [14] A. Dementev, V. Gurentsov, O. Ryazhskaya, and N. Sobolevsky. Production and transport of hadrons generated in nuclear cascades initiated by muons in the rock (exclusive approach). *Nucl. Phys. Proc. Suppl.*, 70:486–488, 1999.

- [15] Davide D'Angelo, for the Borexino collaboration. Seasonal modulation in the Borexino cosmic muon signal. *Proceedings of the 32nd ICRC*, 2011.
- [16] M. Ambrosio, the MACRO Collaboration. High statistics measurement of the underground muon pair separation at gran sasso. *Phys. Rev. D*, 60:032001, Jun 1999.
- [17] M. Ambrosio, the MACRO Collaboration. Measurement of the residual energy of muons in the gran sasso underground laboratories. *Astroparticle Physics*, 19:313–328, 2003.
- [18] J. T. Hong, the MACRO Collaboration. Multiple muon measurements with macro. *hep-ex/9410001*, 1995.
- [19] M. Ambrosio et al, the MACRO collaboration. Vertical muon intensity measured with macro at the gran sasso laboratory. *Phys. Rev. D*, 52:3793–3802, Oct 1995.
- [20] Giuseppe Battistoni, Annarita Margiotta, Silvia Muraro, and Maximiliano Sioli. FLUKA as a new high energy cosmic ray generator. *Nuclear Instruments and Methods in Physics Research Section A: Accelerators, Spectrometers, Detectors and Associated Equipment*, 626-627:S191–S192, 2011.
- [21] S. Ahlen, the MACRO Collaboration. Muon Astronomy with the MACRO Detector. *The Astrophysical Journal*, 412:301–311, 1993.
- [22] Davide D'Angelo, for the Borexino collaboration. Cosmogenic Backgrounds in Borexino. *to.be.published*, 2012.
- [23] M. Selvi. Measurement of muon-induced neutrons with lvd. *presentation at Cosmogenic Activity and Background Workshop, LBNL*, April 2010.
- [24] M. Selvi. Background estimation for Xe1T. *presentation at Cosmogenic Activity and Background Workshop, LBNL*, April 2010.
- [25] S. Abe et al. Production of radioactive isotopes through cosmic muon spallation in KamLAND. *Phys. Rev. C*, 81, February 2010.
- [26] G. Bellini et al, the Borexino collaboration. Muon and Cosmogenic Neutron Detection in Borexino. *Journal of Instrumentation*, 6, 2011.
- [27] G. Alimonti et al, the Borexino collaboration. The Borexino detector at the Laboratori Nazionali del Gran Sasso. *Nuclear Instruments and Methods in Physics Research Section A: Accelerators, Spectrometers, Detectors and Associated Equipment*, 600, 2008.
- [28] A.S. Malgin and O.G. Ryazhskaya. Neutrons from Muons Underground. *Physics of Atomic Nuclei*, 71(10):1769–1781, 2008. Original Russian Text published in *Yadernaya Fizika* (2008, Vol. 71, No. 10, pp. 1800–1811).
- [29] G. Bellini et al, the Borexino collaboration. First evidence of pep solar neutrinos by direct detection in Borexino. *Phys. Rev. Lett.*, 108, 2012.

- [30] N. Agafonova et al, the LVD collaboration. The Measurement of the Total Specific Muon-Generated Neutron Yield Using LVD. *29th International Cosmic Ray Conference*, 9:239–242, 2005.
- [31] Y. F. Wang, V. Balic, G. Gratta, A. Fassò, S. Roesler, and A. Ferrari. Predicting neutron production from cosmic-ray muons. *Phys. Rev. D*, 64, 2001.
- [32] C. Galbiati. *Data Taking and Analysis of the Counting Test Facility of Borexino*. PhD thesis, Università degli Studi di Milano, 1999.
- [33] T. Hagner et al. Muon-induced production of radioactive isotopes in scintillation detectors. *Astroparticle Physics*, 14(1):33–47, 2000.
- [34] H. Back et al, the Borexino collaboration. CNO and pep neutrino spectroscopy in Borexino: Measurement of the deep-underground production of cosmogenic ^{11}C in an organic liquid scintillator. *Phys. Rev. C*, 74, 2006.
- [35] L. Pandola, V. Tomasello, and V. Kudryavtsev. Neutron- and muon- induced background in underground physics experiments. *presentation at: ILIAS 4th Annual Meeting*, 2007.
- [36] Peter D. Meyers, Cristiano Galbiati, Frank P. Calaprice. DarkSide-50: A Direct Search for Dark Matter with New Techniques for Reducing Background. *Proposal, submitted by Princeton to DOE*, April 2011.
- [37] G Alimont, et al, the Borexino collaboration. A large-scale low-background liquid scintillation detector: the counting test facility at Gran Sasso. *NIM A*, 406:411–426, 1998.
- [38] L. Wang et al. Study of Tyvek reflectivity in water. *Chinese Physics C*, 36(7):628–632, 2012.
- [39] M. R. Querry, D. M. Wieliczka, D. J. Segelstein. Handbook of Optical Constants of Solids II. pages 1059–1077, 1991.
- [40] Kevin B. McCarty. *The Borexino Nylon Film and the Third Counting Test Facility*. PhD thesis, Princeton University, 2006.
- [41] Alex W., P. Mosteiro, B. Loer, and F. Calaprice. A Highly Efficient Neutron Veto Using Boron-Loaded Liquid Scintillator. *AIP Conf. Proc.*, 1338:44–48, 2010.
- [42] Peter D. Meyers, Cristiano Galbiati, Frank P. Calaprice. DarkSide-50: A Direct Search for Dark Matter with New Techniques for Reducing Background. *Proposal, submitted by Princeton to DOE*, April 2011.